Photometric variability of MYSOs in the VVV survey

Guilherme Teixeira

Supervisor: **Nanda Kumar**

In collaboration with

Phil Lucas and Leigh Smith, University of Hertfordshire

Stellar evolution

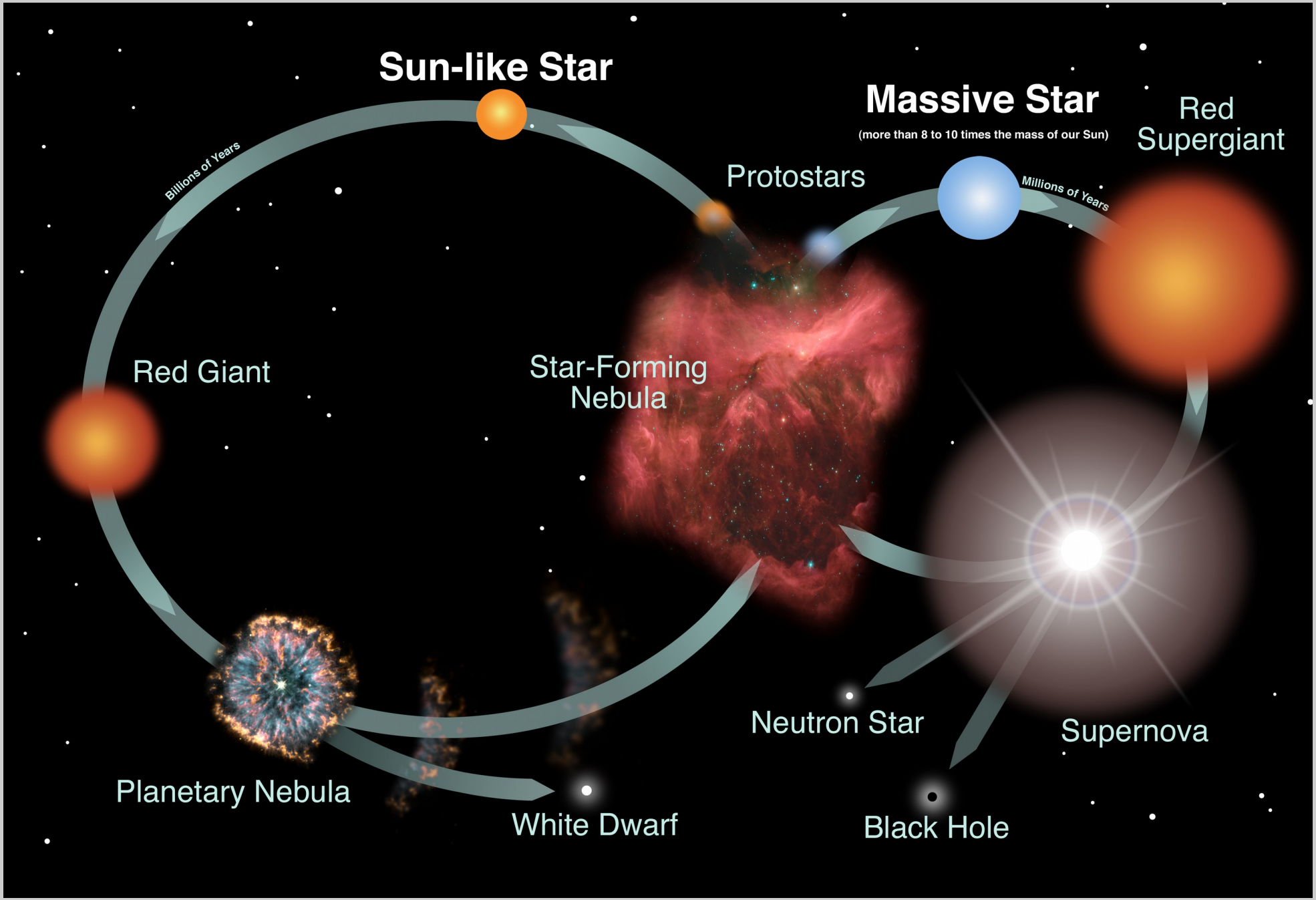

(Credit: NASA and the Night Sky Network)

The HR Diagram

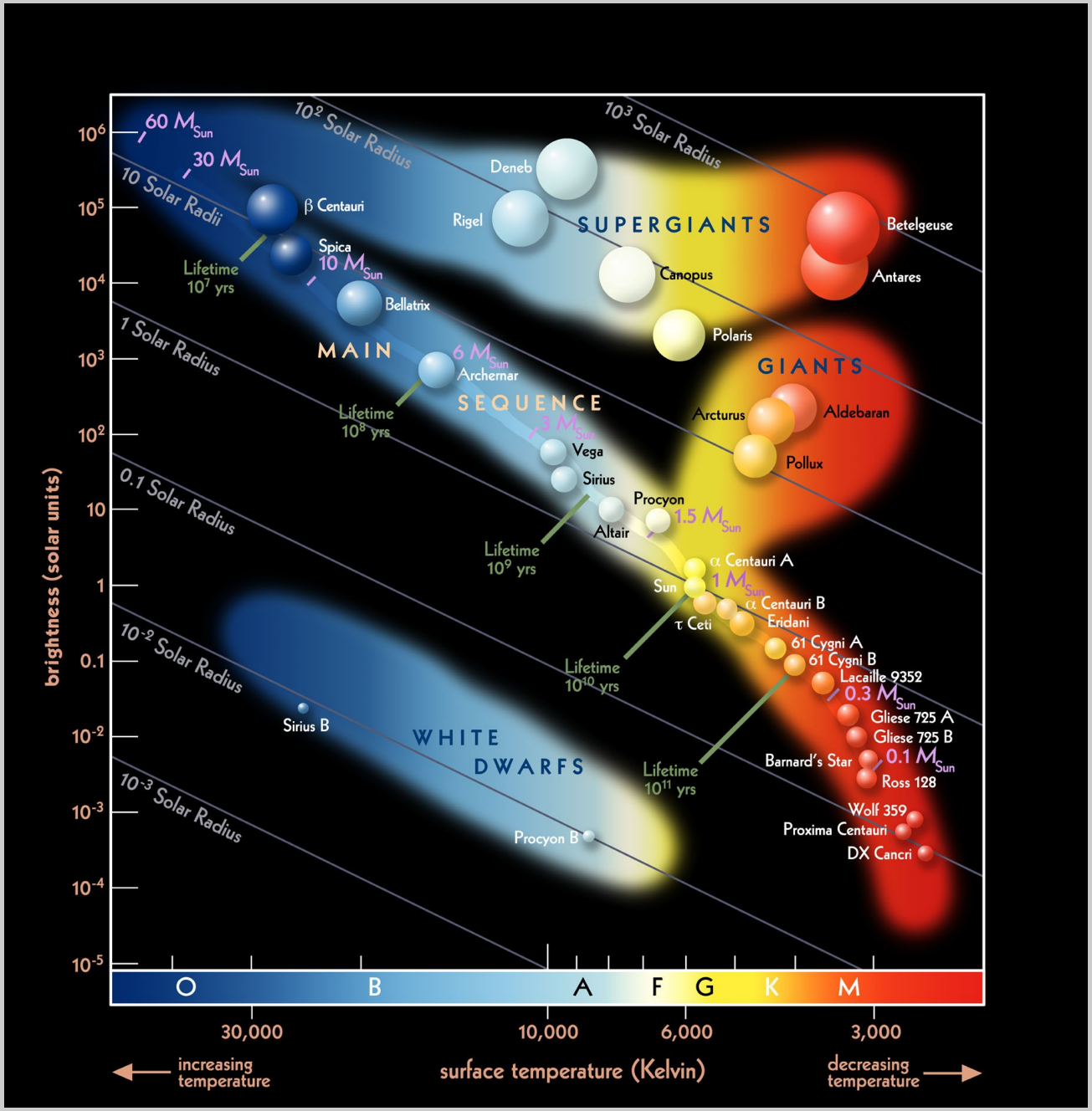

(Credit: ESO)

The HR Diagram - PMS

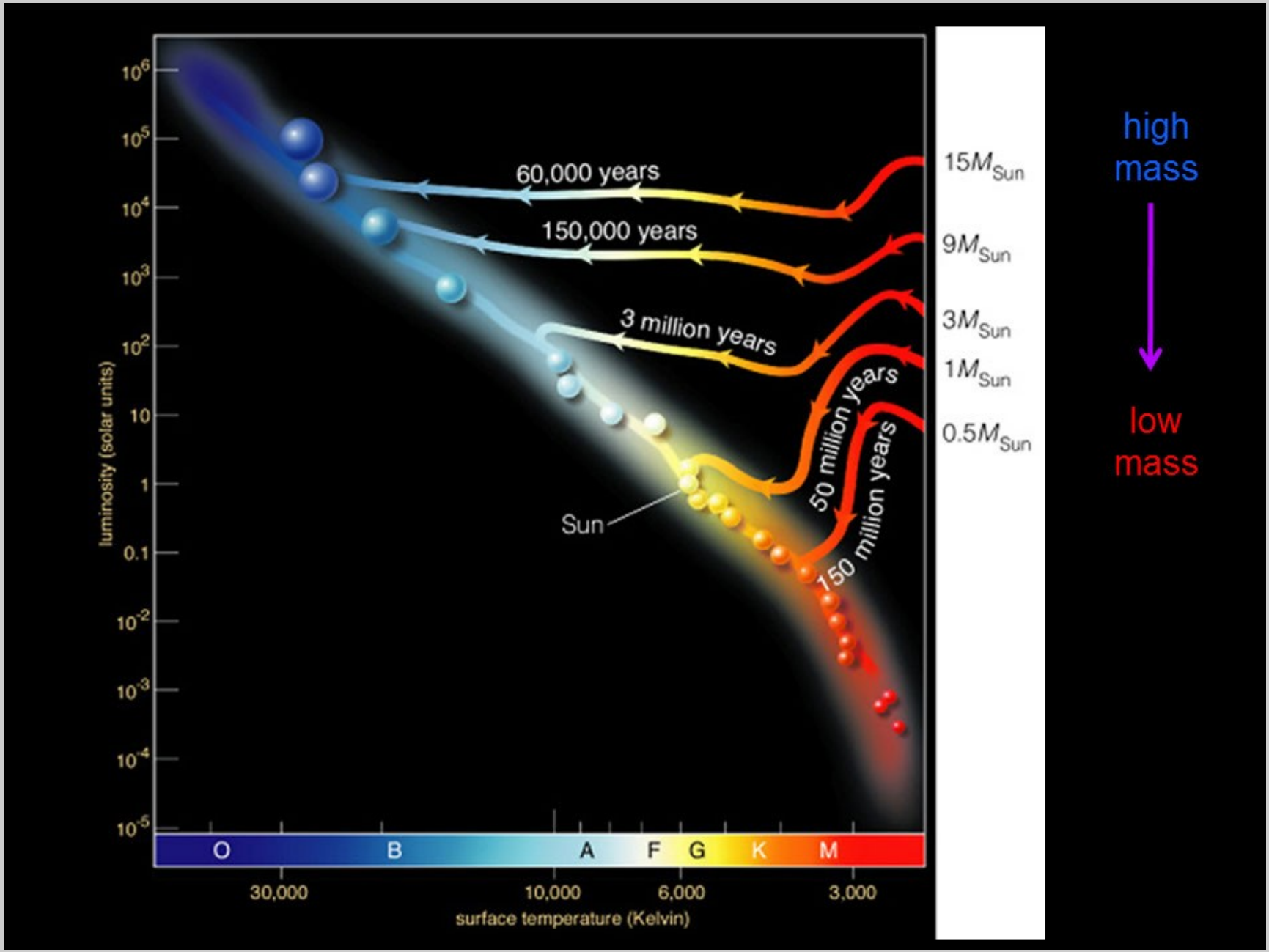

(Credit: Kathryn Z. Hadley)

Star formation – low mass

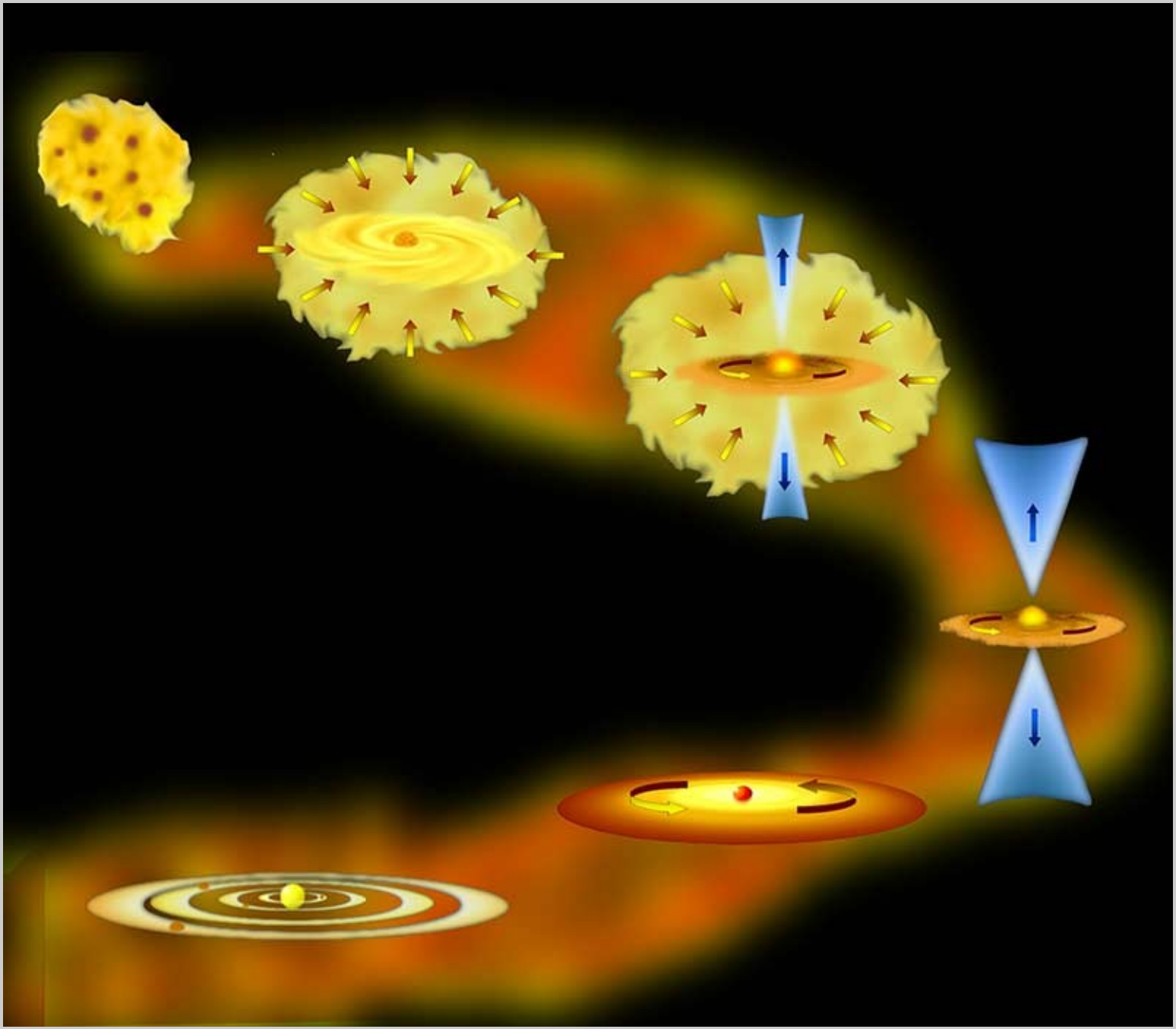

(Credit: Carbonaro & Beltrán)

Star formation – high mass

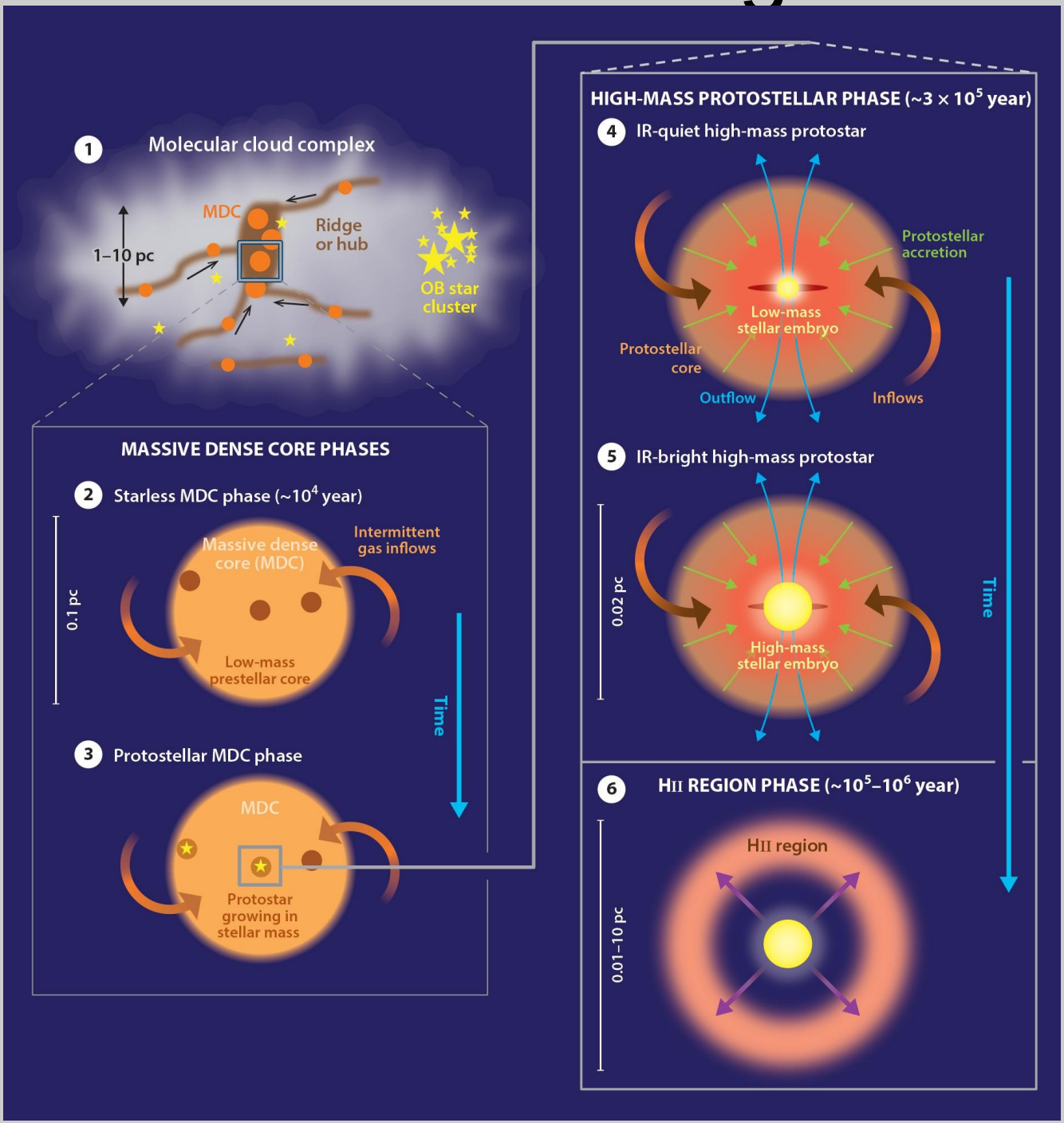

(Credit: Frédérique Motte)

Photometric variability in YSOs

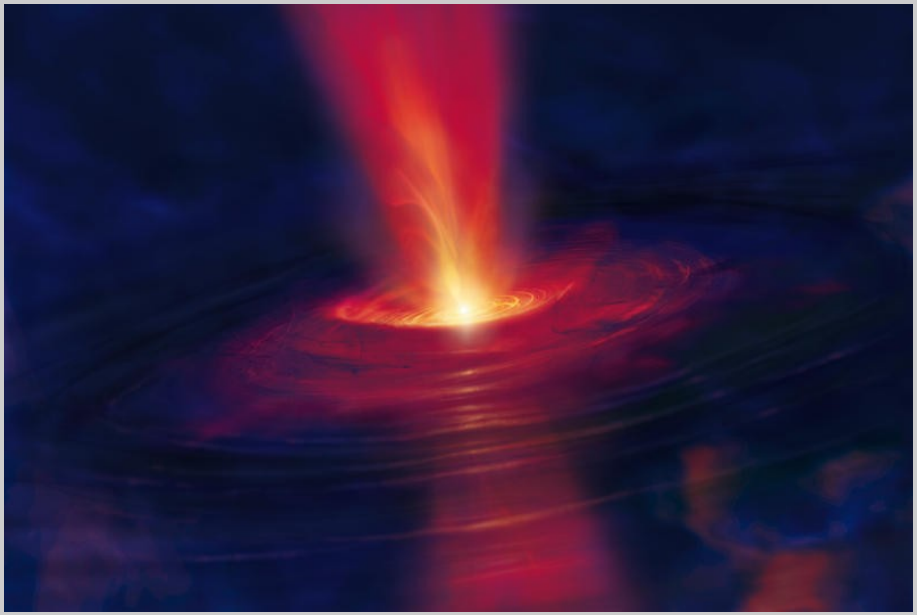

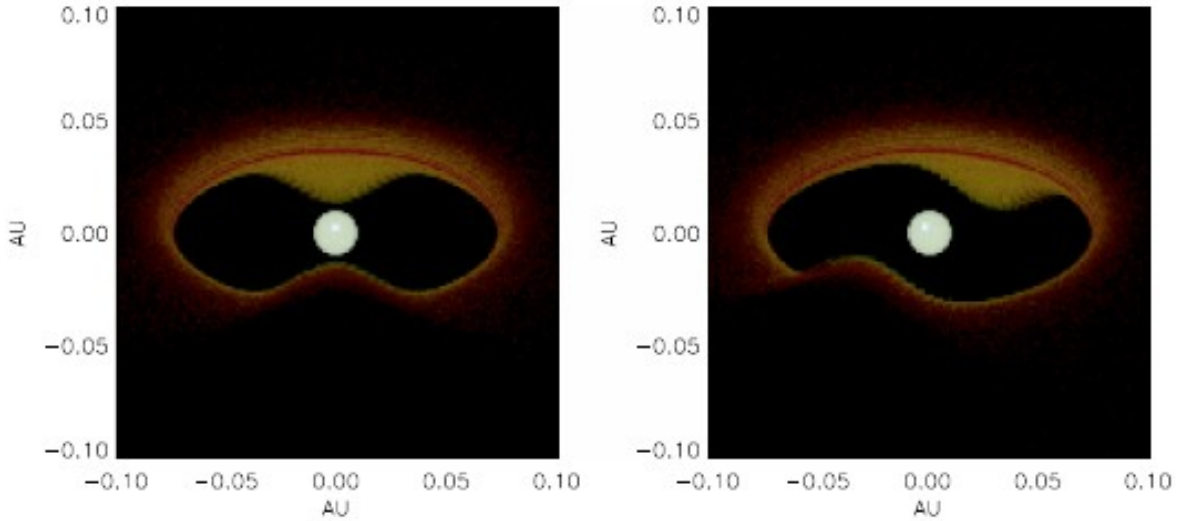

Figure 1. Three-color plots of the star and inner disk region represented by Model 1 having two hot spots due to accretion that illuminate a truncated disk with an inner warp (see Table 1 for details). The disk is inclined at a viewing angle $i = 60°$, and is shown at azimuthal angles $\phi = 0°$ and 20°. The color scale places V band (0.55 μm) as blue, J band (1.2 μm) as green, and IRAC 4.5 μm as red.

(Credit: Kesseli et al.)

VVV survey

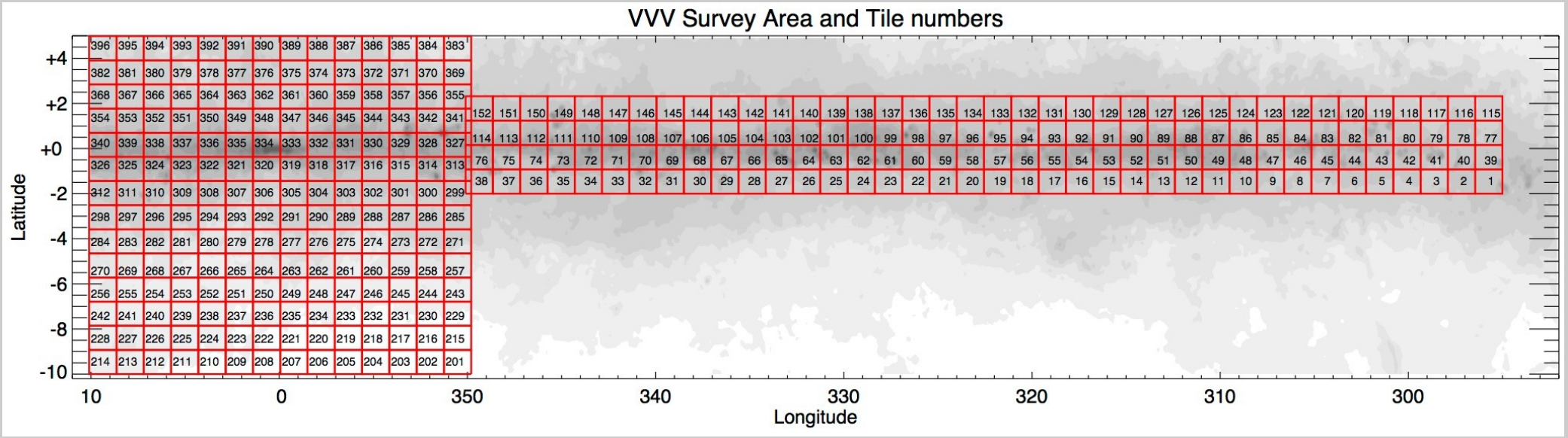

(Credit: D. Minitti et al.)

2μm (K band) multi-epoch imaging photometry between 2010-2015

Sample selection

- 270 Extended Green Objects (EGOs) (153 with VVV counterparts)

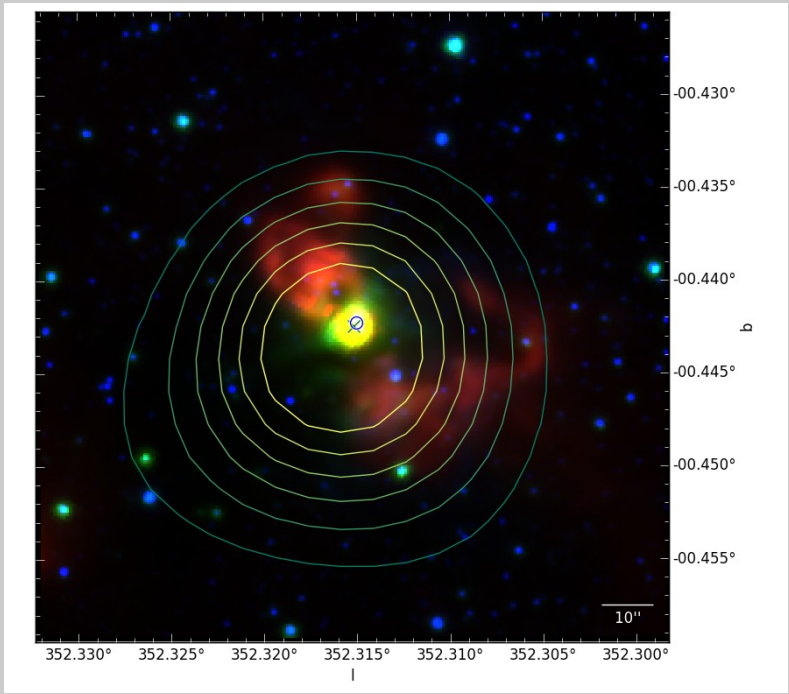

- 574 bright 24 μm with 870 μm peak (non-EGOs) (448 with VVV counterparts)

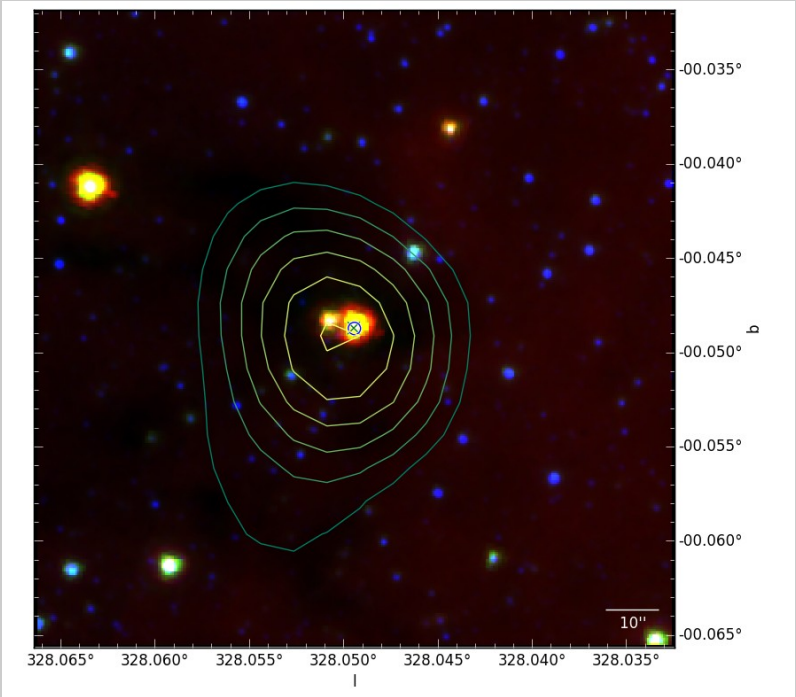

Variability in LCs

Measuring variability

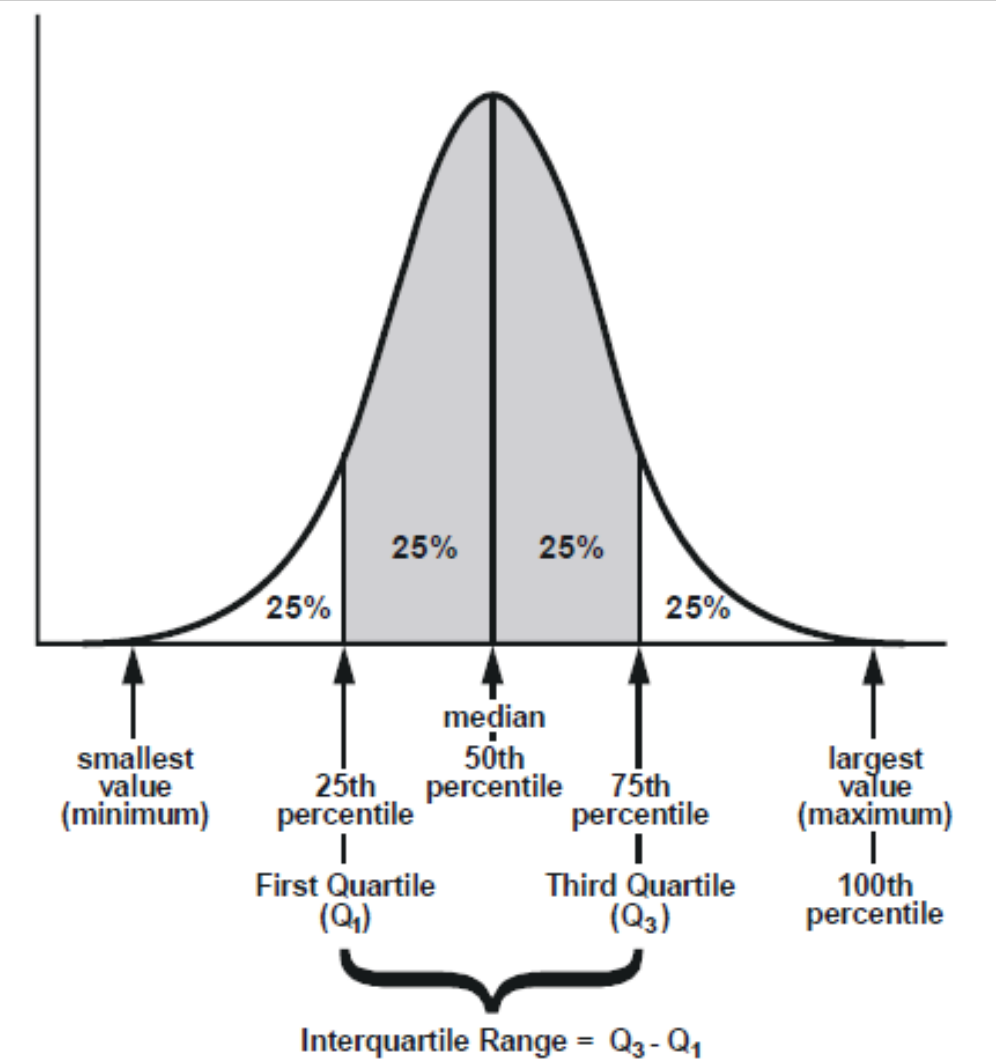

Credit: Kalyan Nandi

$$\Delta K = \max(K_i) - \min(K_i)$$

Variability conditions:

- IQR>0.05
- ΔK>0.15

Variability in LCs

Periodic

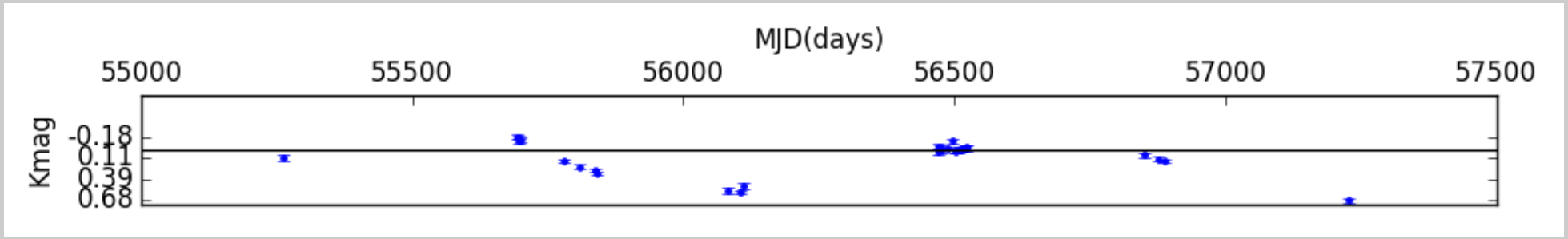

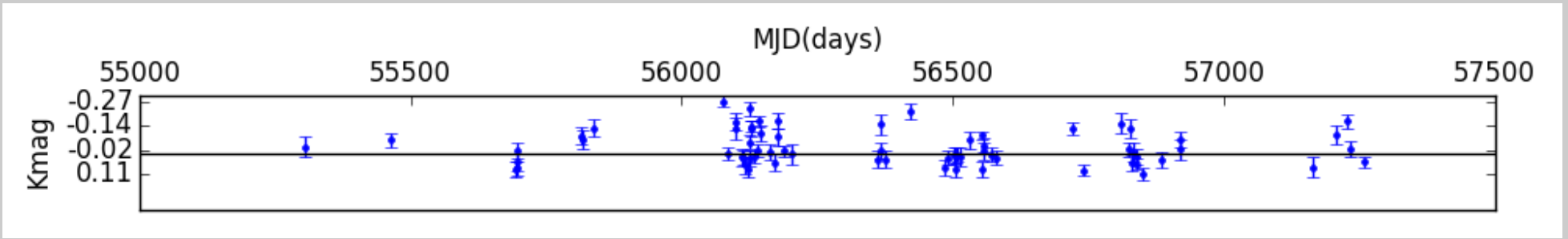

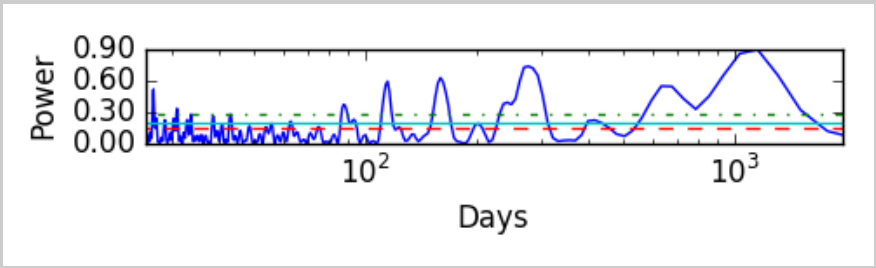

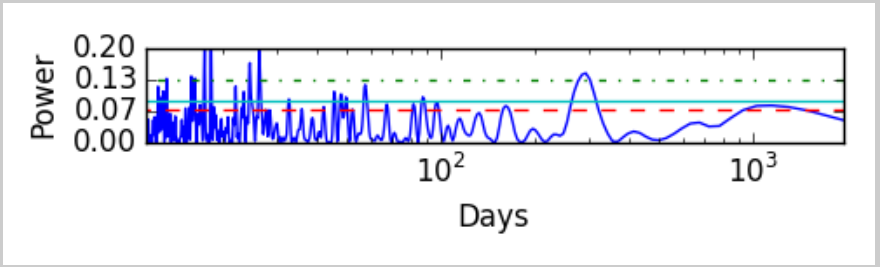

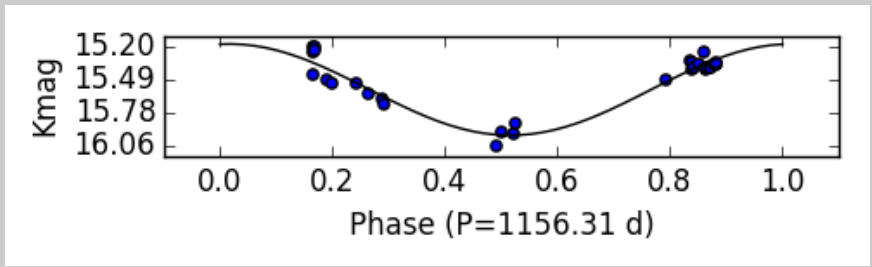

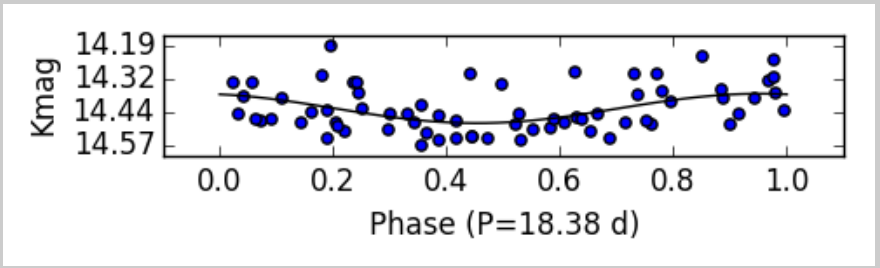

Variability in LCs

Aperiodic

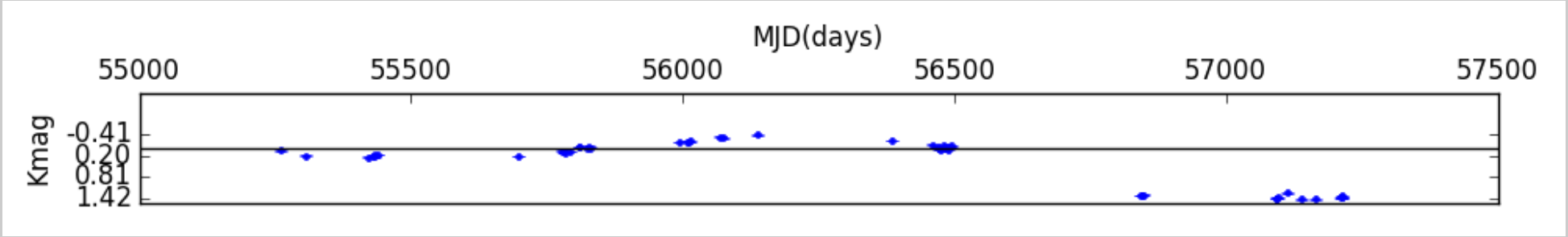

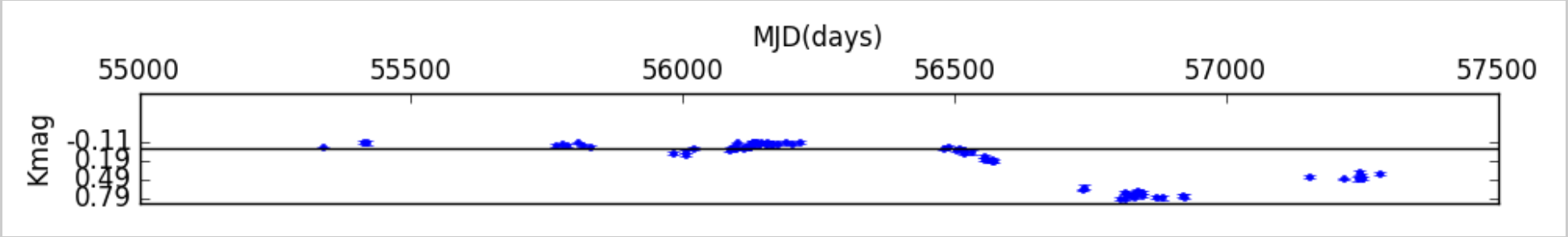

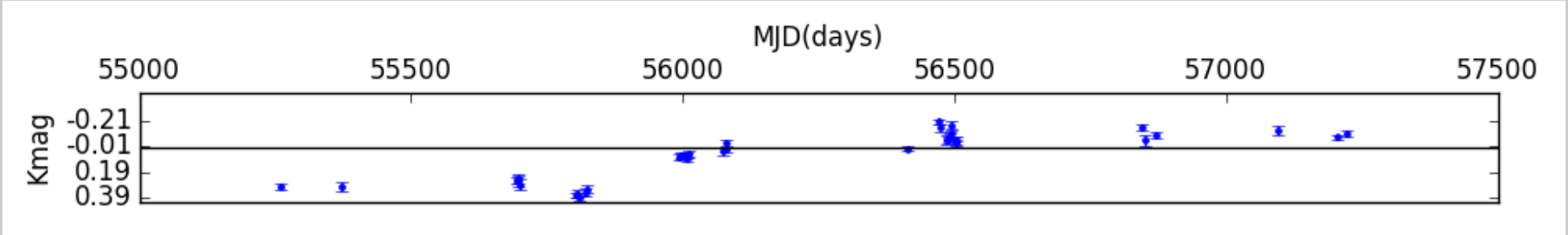

Variability in LCs

Summary

Table 3: Observed parameters of LC classes, for both EGO and non-EGO samples.

LC classification	EGO	non-EGO	Total
Periodic	90 (~ 65%)	21 (~ 41%)	111
Aperiodic	49 (~ 35%)	30 (~ 59%)	79
LPV-yso	53 (~ 38%)	9 (~ 18%)	62
STV	37 (~ 27%)	12 (~ 23%)	49
Dipper	15 (~ 11%)	5 (~ 10%)	20
Fader	13 (~ 9%)	5 (~ 10%)	18
Eruptive	21 (~ 15%)	20 (~ 39%)	41

SEDs

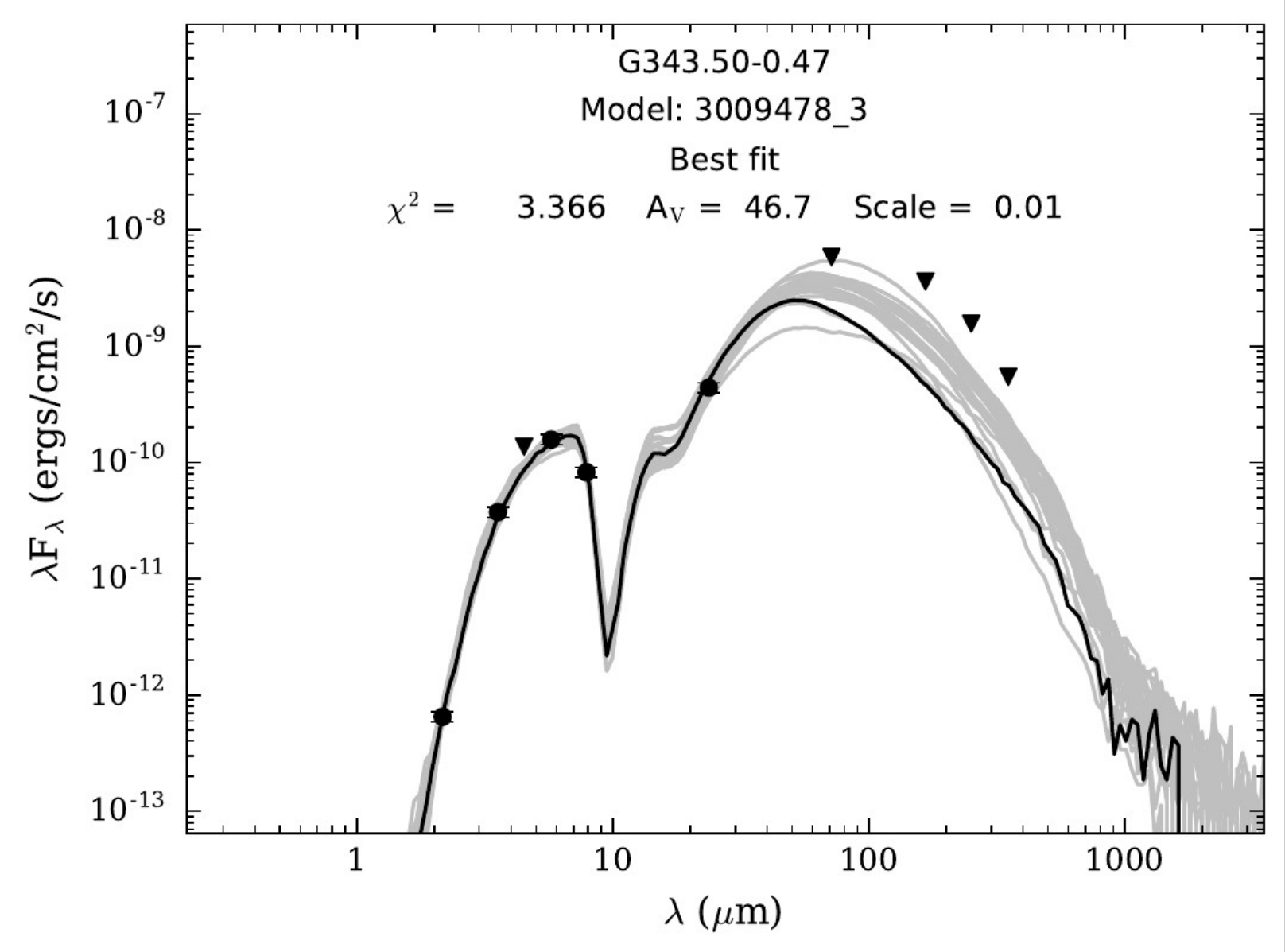
G343.50-0.47
Model: 3009478_3
Best fit
χ^2 = 3.366 A_V = 46.7 Scale = 0.01
λF_λ (ergs/cm^2/s)
10^{-7}
10^{-8}
10^{-9}
10^{-10}
10^{-11}
10^{-12}
10^{-13}
1
10
100
1000
λ (μm)

SEDs

Summary

Table 4: SED results by mass bin.

M ($M_\odot$) Range	Sources (%) Ratio	L ($L_\odot$) Range	L ($L_\odot$) Median	$\dot{M}_{env}$ ($M_\odot\ yr^{-1}$) Range	$\dot{M}_{env}$ ($M_\odot\ yr^{-1}$) Median	$A_{V_{circum}}$ Range	$A_{V_{circum}}$ Median
$M < 4$	~ 59	[4.0E-1,9.0E2]	5.0E1	[0,4E-4]	1.3E-5	[6E-1,6E5]	74
$4 \leq M < 6$	~ 21	[8.8E1,1.2E3]	2.9E2	[0,4E-4]	7.8E-5	[2E0,2E4]	56
$6 \leq M < 8$	~ 14	[2.9E2,5.1E3]	9.3E2	[0,6E-4]	2.0E-4	[5E0,1E5]	66
$8 \leq M$	~ 6	[1.3E3,3.7E4]	3.0E3	[1E-4,4E-3]	2.8E-4	[4E1,4E5]	228

Table 5: Summary of the median fit parameters, for both EGO and non-EGO samples divided by periodicity.

Parameter	EGO	non-EGO	Periodic	Aperiodic
ΔK_s (mag)	0.52	1.02	0.58	0.69
Period (days)	312	416	126	-
M ($M_\odot$)	3.2	3.8	3.2	3.6
$\dot{M}$ ($M_\odot\ yr^-1$)	4E-5	6E-6	4E-5	2E-5
$\dot{M}_{disk}$ ($M_\odot\ yr^-1$)	3E-7	7E-7	3E-7	6E-7
L ($L_\odot$)	125	212	125	190
Age (Myr)	5.0	5.6	5.0	5.0
T (K)	4841	7795	4857	5990
$A_{V_{circum}}$	61	125	71	54

HR diagram

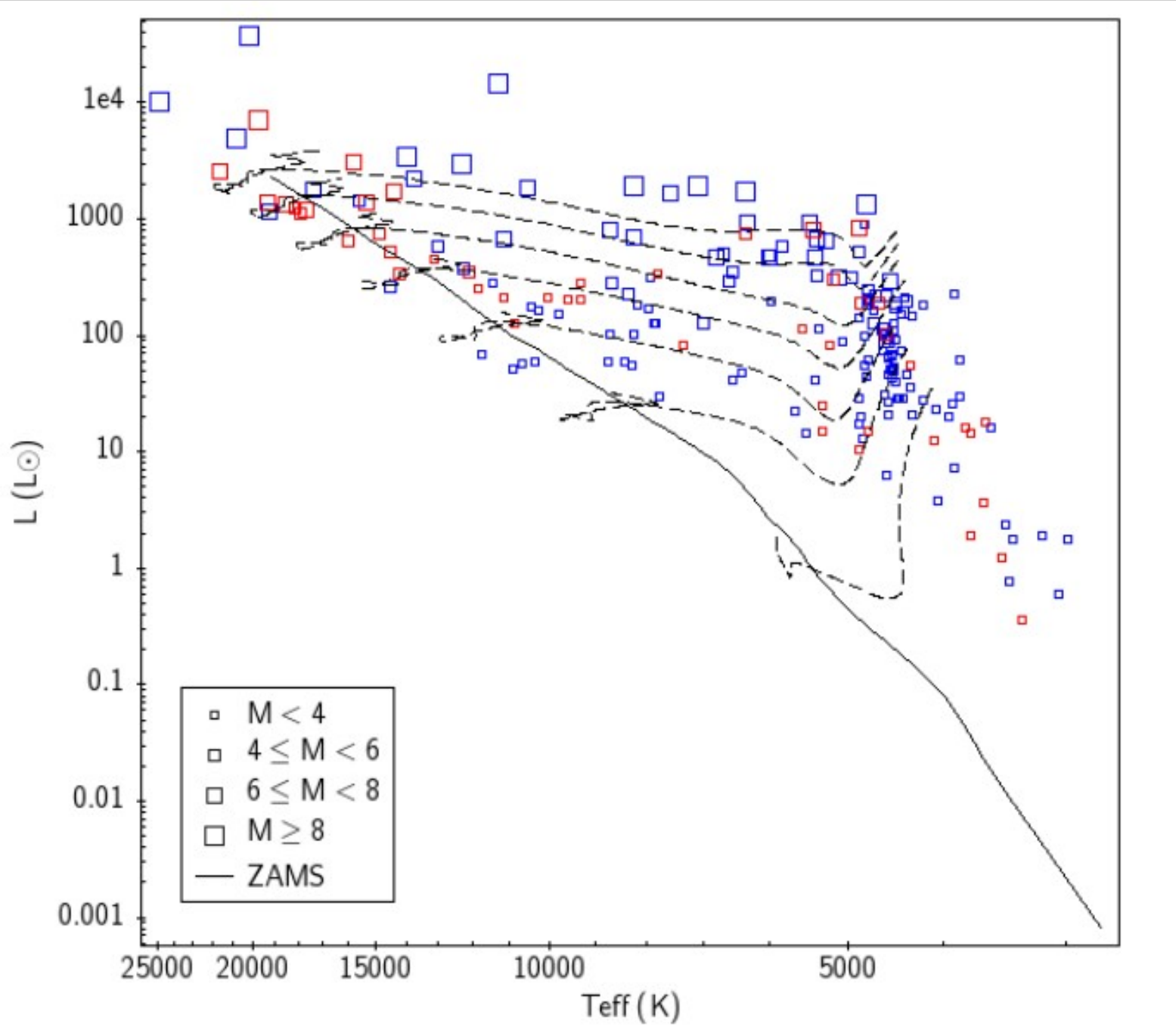
1e4
1000
100
10
1
0.1
0.01
0.001
L (L⊙)
25000
20000
15000
10000
5000
Teff (K)
M < 4
4 ≤ M < 6
6 ≤ M < 8
M ≥ 8
ZAMS

Summary

- 190 MYSO candidates (139 EGOs and 51 non-EGOs) are NIR variable (IQR > 0.05 & ΔK>0.15 mag)
- 111 were classified as periodic and 79 as aperiodic
- SED models show 47 sources as M>4 Msun and 6 as M>8 Msun
- On an HR diagram most low mass EGOs are close to the birth-line
- High rate of variable EGOs implies a NIR variability in MYSOs linked to accretion phenomena and outflow activity
- Our selection criteria for non-EGOs ensures good MYSO candidates but may lead to the exclusion of the most luminous FIR sources and counterparts which will be analized in a future work

Possible models(?)

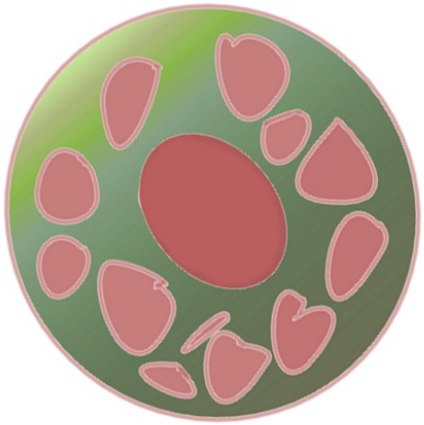

Non-EGOs

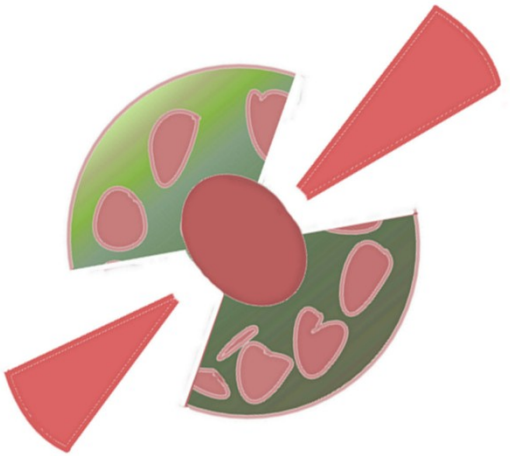

EGOs

Bloated and fluffy protostars

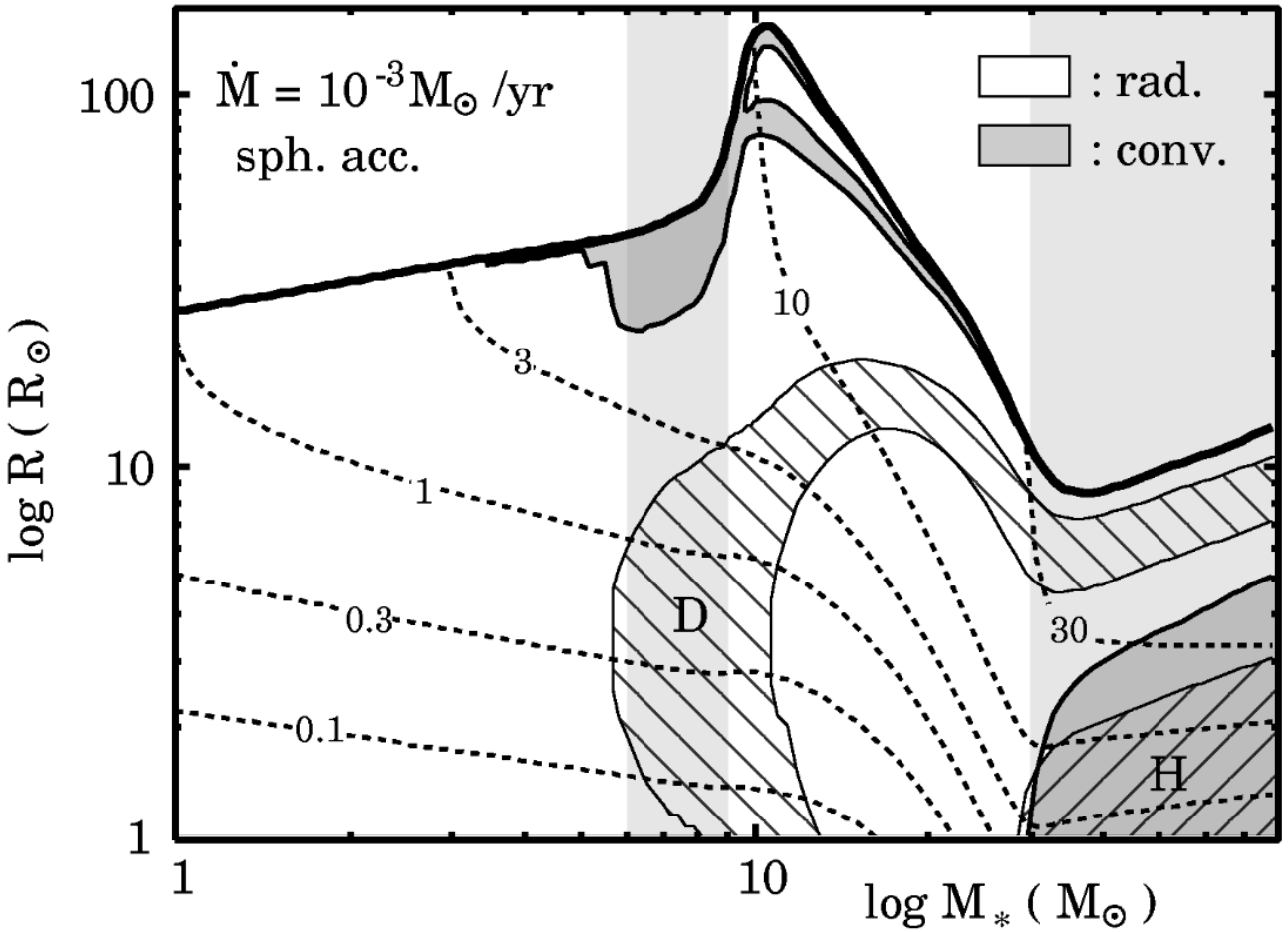

The Astrophysical Journal, 721:478–492, 2010 September 20

EVOLUTION OF MASSIVE PROTOSTARS VIA DISK ACCRETION

Takashi Hosokawa[1,2,3], Harold W. Yorke[2], and Kazuyuki Omukai[1,3]

The Astrophysical Journal, 691:823–846, 2009 January 20

EVOLUTION OF MASSIVE PROTOSTARS WITH HIGH ACCRETION RATES

Takashi Hosokawa and Kazuyuki Omukai

About the absence of a proper zero age main sequence for massive stars

P.A. Bernasconi and A. Maeder

Geneva Observatory, CH-1290 Sauverny, Switzerland

Received 1 June 1995 / Accepted 1 August 1995

Abstract. The formation of stars up to 120 $M_\odot$ is computed in the framework of the accretion scenario. For realistic accretion rates derived from the observed line width in various molecular dark clouds, the accretion interlude lasts some 2-2.5 Myr, and accounts for an appreciable nuclear evolution during the optically thick MS life. Several new results are found concerning massive stars at the top of the MS: 1) A newly formed massive star with $M \geq 40\ M_\odot$ at the time it emerges from its parental cloud has already burned a substantial fraction of its central hydrogen content. 2) As a consequence, the formal MS lifetime is substantially reduced. 3) A proper ZAMS does not exist, since at the time it becomes visible, the star has already evolved towards lower T_{eff}. 4) As a result of previous evolution, the size of the convective core for a given central H content is reduced by about 5-10 %. 5) We find that for realistic accretion rates applicable to ordinary star forming regions in the Galaxy and Magellanic Clouds, a truncation of the IMF is naturally established around 85-150 $M_\odot$ where the accretion time becomes comparable to the hydrogen burning time. 6) Since massive stars spend a fraction of their H-burning phase in the parental cocoon, their true number is larger than estimated and the slope of the IMF is flatter.

$10^3 - 10^4$ cm^{-3} in the innermost regions, the volume of a cloud concerned by the formation process of a 1 $M_\odot$ star encompasses at most 0.05-0.1 pc, the size reaching 1.5 pc for extreme massive stars (Myers & Fuller 1992, MF hereafter; see also Sect. 2). It is within this volume that matter is believed to organize itself in spatially thin, several hundred AU extended disks, whose viscous torque eventually leads to a radial, two dimensional flow supplying the newly formed central protostella core with unprocessed material.

The early evolution of low to intermediate mass protostellar cores during the main accretion phase has been thoroughly investigated by Stahler et al. (1980a, b, 1981) and Palla & Stahler (1991, 1992, 1993). These authors showed the photospheric properties of the accreting models to follow a characteristic evolutionary path (the birthline) mainly directed by the thermostatic action of deuterium burning in an initial fully convective interior. Contrarily to the hydrodynamical simulations of a spherically symmetric, collapsing isothermal cloud performed by Larson (1969, 1972), their birthline well matches the upper envelope for TTauri stars in the Hertzprung-Russel (HR) diagram (Stahler 1983) and fits correctly the observed position of their intermediate mass counterparts. Herbig Ae and Be stars (Palla & Stahler

An IRDC, a neat clump, and highly variable YSO

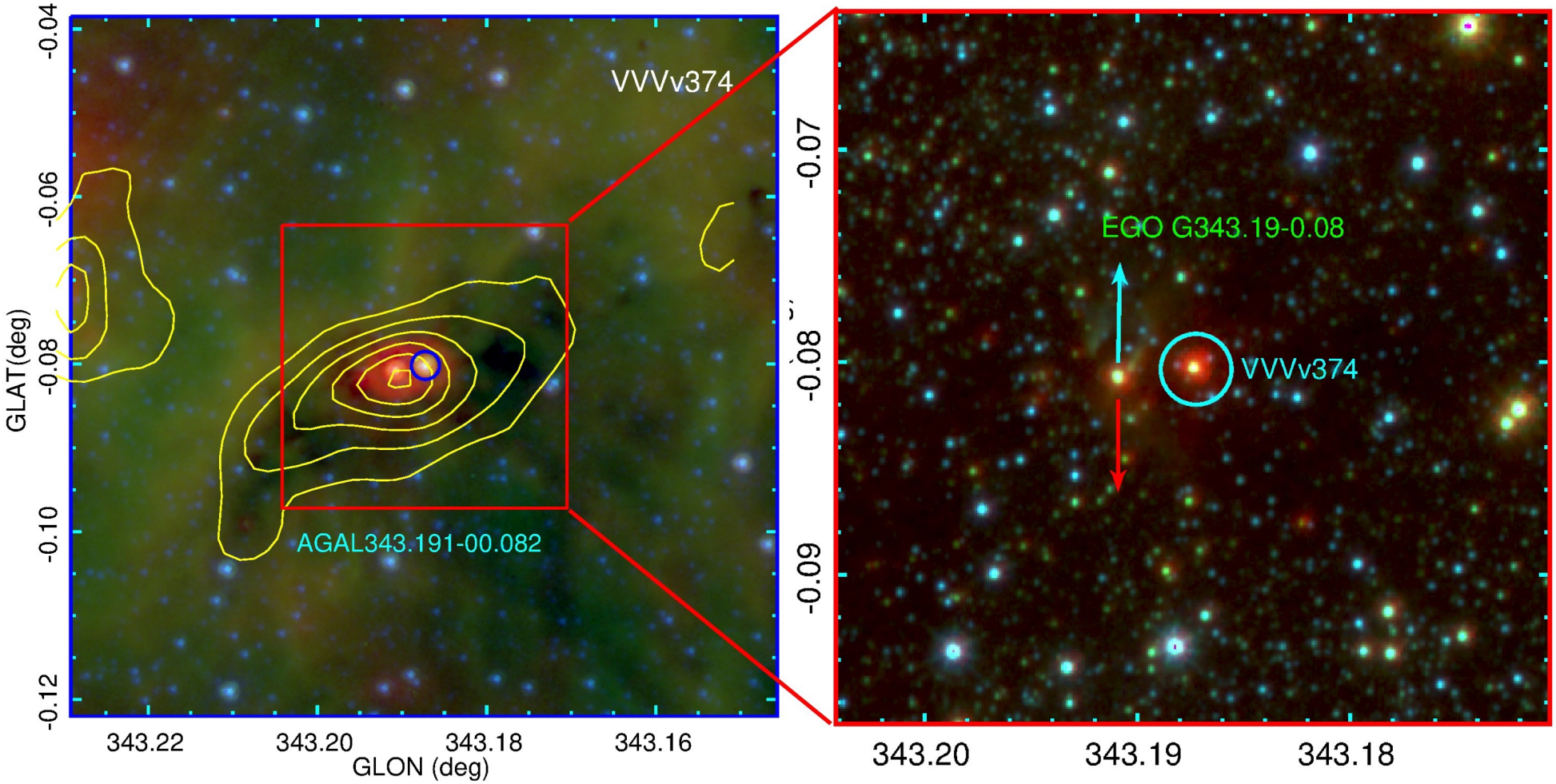

Highly-variable (ΔK>1mag) point sources in ATLASGAL clumps
Kumar, Contreras-Pena, Lucas & Thompson, 2016, ApJ,833,24

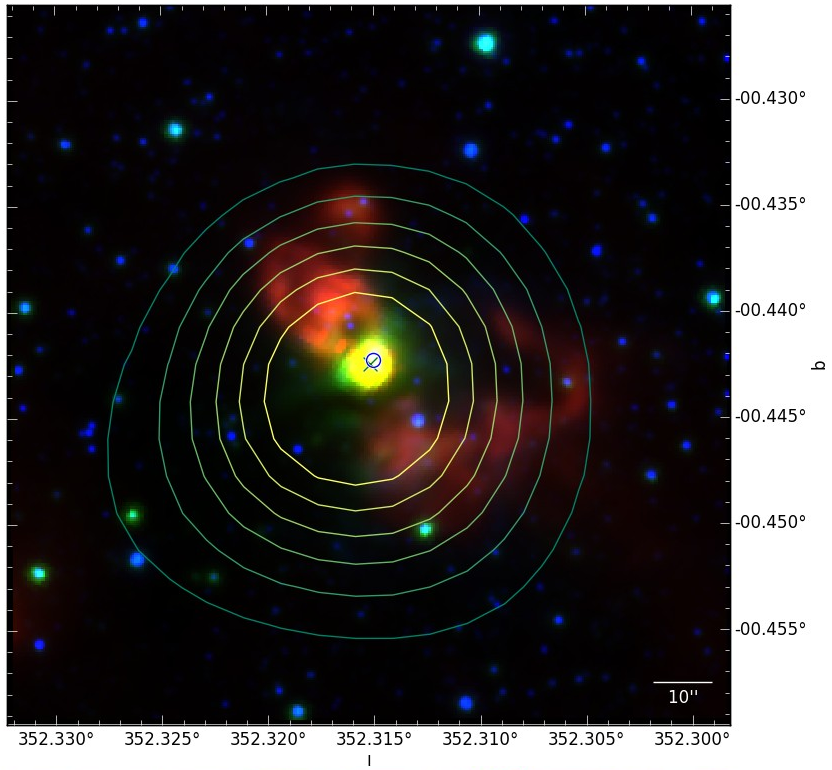
-00.430°
-00.435°
-00.440°
-00.445°
-00.450°
-00.455°
b
10''
352.330°
352.325°
352.320°
352.315°
352.310°
352.305°
352.300°
l

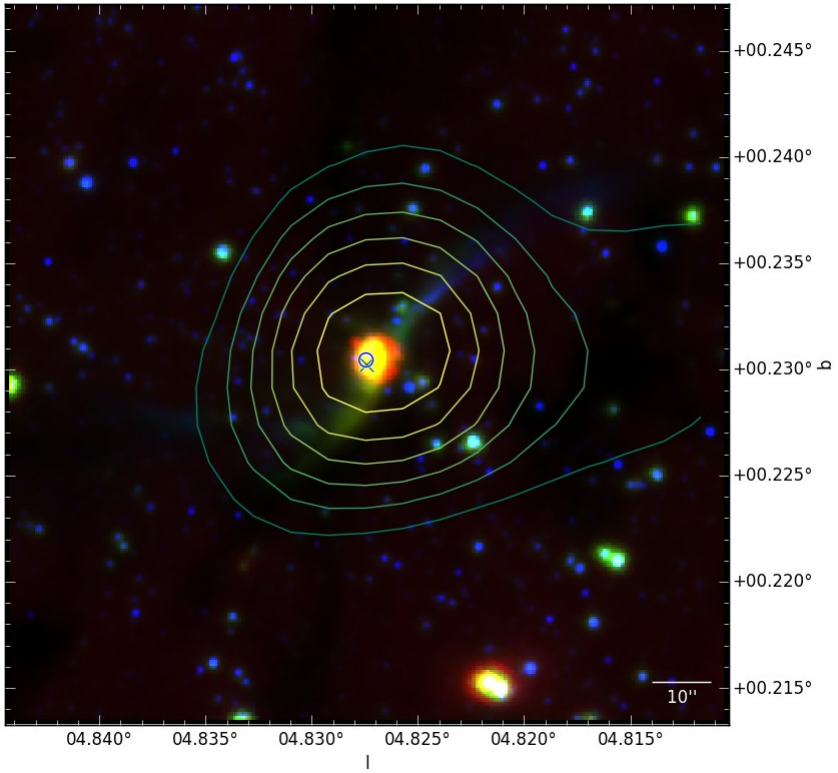
+00.245°
+00.240°
+00.235°
+00.230°
+00.225°
+00.220°
+00.215°
b
10''
04.840°
04.835°
04.830°
04.825°
04.820°
04.815°
l

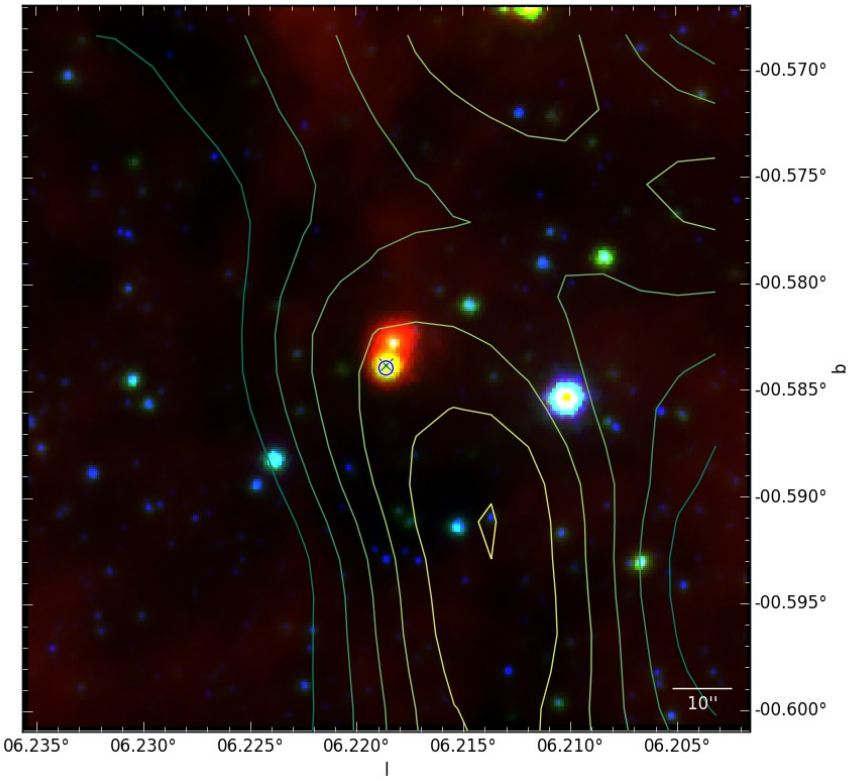
-00.570°
-00.575°
-00.580°
-00.585°
-00.590°
-00.595°
-00.600°
b
10''
06.235°
06.230°
06.225°
06.220°
06.215°
06.210°
06.205°
l

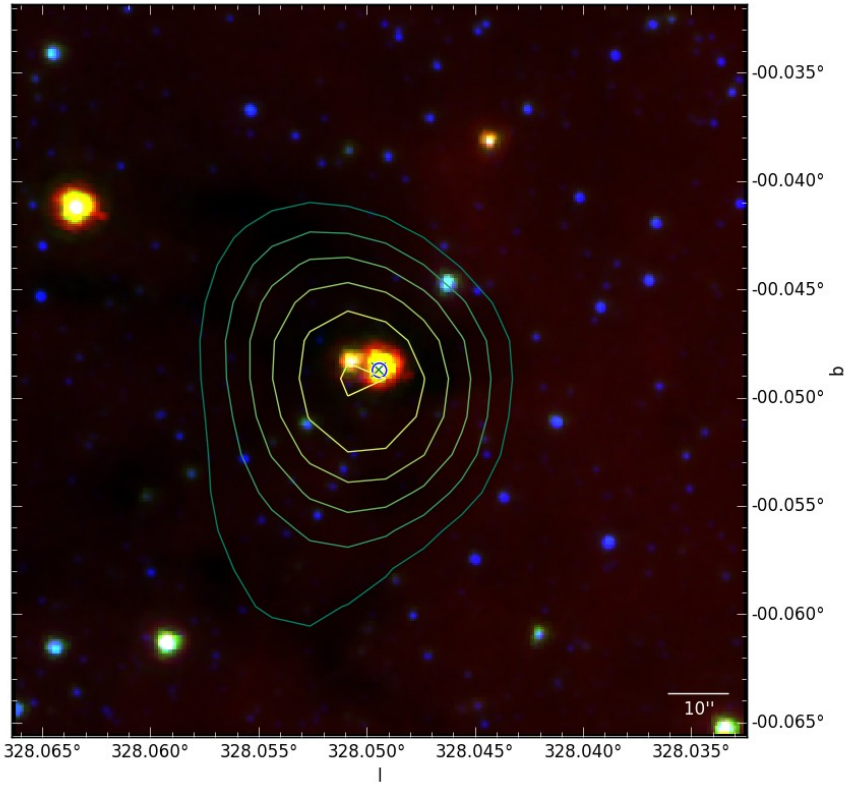
-00.035°
-00.040°
-00.045°
-00.050°
-00.055°
-00.060°
-00.065°
b
10''
328.065°
328.060°
328.055°
328.050°
328.045°
328.040°
328.035°
l

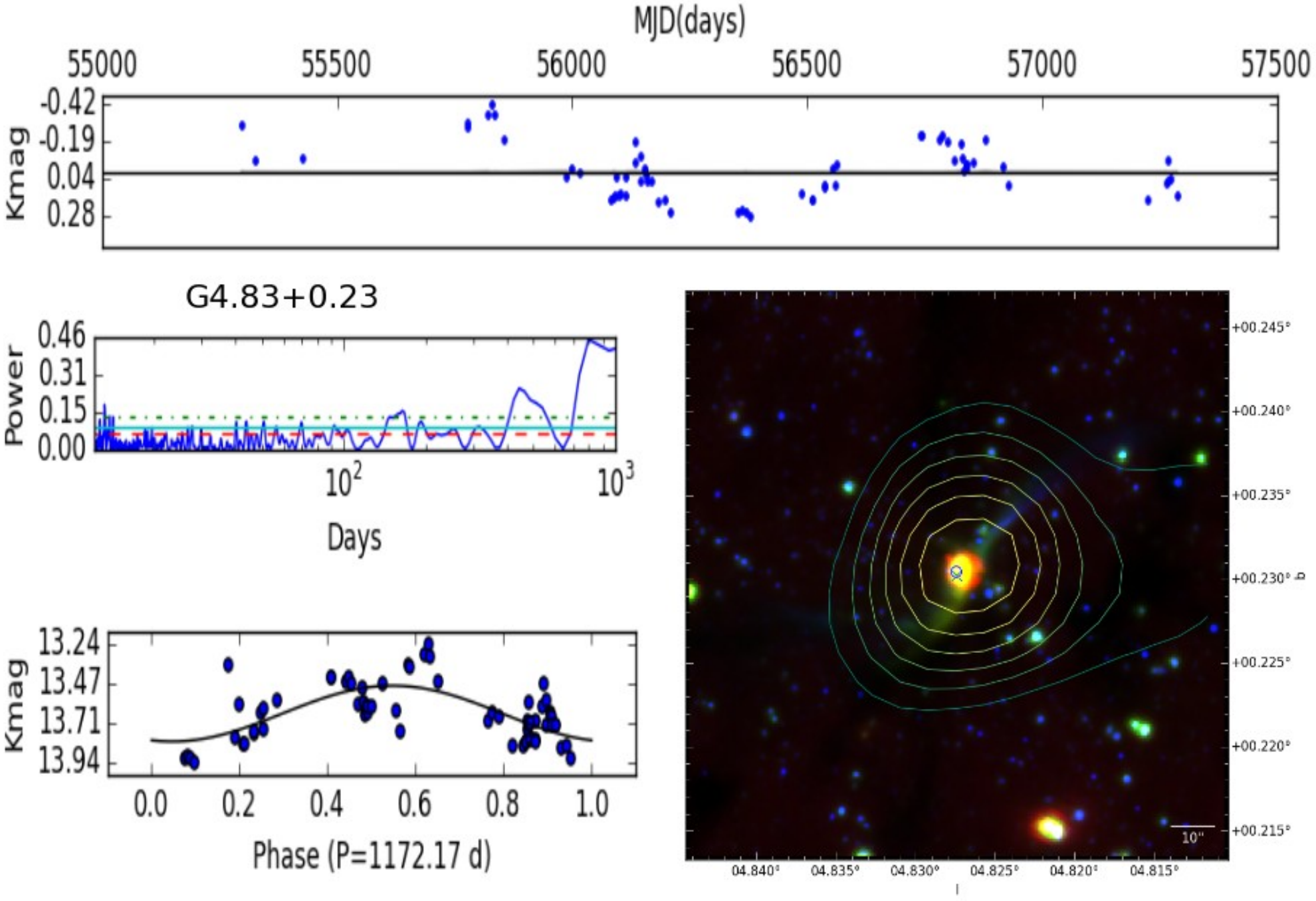
MJD(days)
55000
55500
56000
56500
57000
57500
Kmag
-0.42
-0.19
0.04
0.28
G4.83+0.23
Power
0.46
0.31
0.15
0.00
10^2
10^3
Days
Kmag
13.24
13.47
13.71
13.94
0.0
0.2
0.4
0.6
0.8
1.0
Phase (P=1172.17 d)
+00.245°
+00.240°
+00.235°
+00.230°
+00.225°
+00.220°
+00.215°
10''
04.840°
04.835°
04.830°
04.825°
04.820°
04.815°